Overview of Recen t Results from the Alcator C-Mod Tokamak[*]

E. Marmar, P . Acedo[a], O. Batishc hev, R. Bengtson,[b] R.L. Boivin, F. Bom barda,[c] X. Bonnin,[b] P. Bonoli, C. Bosw ell, R. Bra venec,[b] N. Bretz,[d] C. Chang,[n] C. Christensen, G. Cima,[d] W. Dorland,[d] J. Drake,[e] E. Eisner,[b] G. Esser,[f] M. Fink enthal,[g] C. Fiore, K. Fournier,[h] T. Fredian, R. Gandy ,[i] S. Gangadhara, K. Gen tle,[b] J. Goetz, R. Granetz, M. Green wald, H. Griem,[e] G. Halloc k, J. Harker,[b] J. Heard,[i] J. Hosea,[d] A. Hubbard, I. Hutc hinson, J. Irby, D. Johnson,[d] J. Ke, J. Kesner, S. Krasheninnik ov, B. LaBom- bard, H. Lamela,[a] B. LeBlanc,[d] Y. Lin, B. Lipsc hultz, S. Lisgo,[j] R. Maqueda,[k] M. Ma y,[g] A. Mazurenk o, S. Migliuolo, E. Nelson-Melb y, G. Miller, D. Mossessian, R. Nat rieb,[h] R. Nazikian,[d] R. Neu,[l] H. Ohk awa, P. O'Shea, T.S. P edersen, D. P appas, C.K. Phillips,[d] A. Pigaro v, C.S. Pitcher, M. P orkolab, J. Ramos, J. Reardon, J. Rice, B. Rogers,[e] J.C. Rost, W. Ro wan,[b] J. Schachter, G. Schilling,[d] H. Scott,[h] C. Skinner,[d] J.A. Snipes, V. Soukhanovskii,[g] P. Stangeby,[j] P. Stek, J. Stillerman, Y. T akase, G. T aylor,[d] J. Terry, T. Tutt, M. Umansky, W. Wampler,[m] A. W an,[h] C. W atts,[i] L. W eathers, J. W eaver,[e] B. W elch,[e] J.R. Wilson,[d] S. W olfe, K.-L. W ong,[d] A. W ootton,[b] S. W ukitch, G. W urden,[k] Y. In, H. Y uh, S. Zweben[d]

MIT Plasma Science and F usion Center[*], Cam bridge, MA 02139, USA

[a]Carlos III Univ ersity, Madrid, Spain, [b]U. Texas, Austin, TX, USA, [c]ENEA F rascati, Italy, [d]Princeton Plasma Ph ysics Lab., Princeton, NJ, USA, [e]U. Maryland, College Park, MD, USA, [f]KFA Julich, German y, [g]Johns Hopkins U., Baltimore, MD, USA, [h]Lawrence Livermore National Lab., Liv ermore, CA, USA, [i]Auburn U., Auburn, AL, USA, [j]U. T oronto, Toronto, On tario, Canada, [k]Los Alamos National Lab., Los Alamos, NM, USA, [l]MPIPP , Garching, German y, [m]Sandia National Lab., Albuquerque, NM, USA , [n]Courant Institute of Mathematical Sciences, New Y ork University, New Y ork, NY, USA

Abstract

Recent results from the compact, high field, Alcator C-Mod tokamak program are summ arized. H-mode threshold studies ha ve demonstrated that the threshold appears to be closely related to local edge plasma parameters: for fixed field and plasma cur- rent, $T_e(\psi_{95})$ takes on a density independent value at the transition. The Enhanced D-Alpha H-Mode (EDA) regime has been in vestigated. EDA is distinct from ELM free H mode, in that there is no accum ulation of impurities, and at the same time EDA does not exhibit large discrete ELMs. The energy confinemen t is degraded by only about 10%, compared to ELM free. Comparisons for EDA with ELMy H-Mode database scal- ings indicate $\tau_{EDA} \sim 1.2\tau_{ITER97H}$. Strong toroidal rotation is observed in ICRF-only auxiliary heated plasmas; the rotation increases with plasma pressure, and decreases with increasing plasma curren t. The inferred radial electric field reaches the order of $30\,kV/m$ near the center of the plasma. Through feedbac k controlled nitrogen impurit y

---

puffing, steady state detached EDA H-Modes have been achieved with $Z_{eff} < 1.5$. τ_E is reduced by about 10% in the detached case, compared to the confinement before the N_2 puff begins. The heat load to the divertor is reduced by a factor of 4. Volume recombination rates are measured in the divertor, using 2-d tomography of Balmer series TV movies. Volume recombination can be a significant contributor to the overall reduction in ion current to the divertor plates which occurs in detachment. Particle balance measurements indicate that the divertor and main chamber plasmas are largely isolated from one another, at least with regard to particle recycling, with most of the main chamber (core plus scrape-off) fueling coming from neutrals in the main chamber volume. With the addition of Lower Hybrid Current Drive, C-Mod would be an ideal vehicle for investigation of advanced tokamak operation with fully relaxed current profiles. Detailed modeling indicates that discharges approaching the β limit ($\beta_N \sim 3.7$) with > 70% bootstrap fraction should be achievable.

1. INTRODUCTION

There are four key areas of investigation on the compact, high magnetic field, Alcator C-Mod tokamak[1]. Transport studies on C-Mod provide critical tests of empirical scalings and theoretically-based interpretations of tokamak transport at unique dimensional parameters, but with dimensionless parameters comparable to those in larger experiments. Divertor research on C-Mod takes advantage of the advanced divertor shaping, very high scrape-off layer power density, high divertor plasma density, unique abilities in diagnosis and neutral control, and a high-Z metal wall. Ion cyclotron radio frequency power provides the auxiliary heating on C-Mod, and is exploited for research into wave absorption and parasitic losses and mode conversion processes. Advanced tokamak research on C-Mod proposes demonstrating fully relaxed current profile control and sustainment through efficient off-axis current drive by Lower Hybrid waves.

2. TRANSPORT

In the area of transport research, we have continued investigations of the L/H threshold, with emphasis on local measurements[2]. Trends demonstrating an edge temperature threshold have been elaborated. Figure 1 indicates that $T_e(\psi_{95})$ shows a much tighter correlation with confinement mode than does the global parameter, total input power (P_{tot}). Subtracting the radiated power from (P_{tot}) does not significantly decrease this scatter. These data, which are for a series of discharges with $B_\phi = 5.3\,T$ and $I_p = 0.8\,MA$, show a clear edge temperature threshold of about 120 eV. Scans for $B_\phi = 8\,T$ show a similar result, but with an increased threshold, at about 220 eV. In both cases, the threshold temperature approximately doubles when the $B \times \nabla B$ direction is reversed so that the ion drift direction is away from the divertor. We have compared our data with the threshold theory of Rogers and Drake,[3] and the results are shown in figure 2. The theory, which is based on electromagnetic suppression of turbulence, via self generated $E \times B$ flow combined with $B \times \nabla B$ diamagnetic flow, predicts that the L to H transition should occur when the edge parameters are such that $\alpha = -Rq^2 d\beta/dr > 0.5$ and $\alpha_{di} = \rho_s c_s t_o/L_o L_p > 0.6$ (ρ_s is the ion gyroradius, c_s is the ion sound speed, t_o is the ideal ballooning growth time, L_o is the ballooning

spatial scale, and L_p is the pressure scale length. The boundary between L and H mode is in very good qualitative agreement with the theory, with both α and α_{di} at the experimental threshold being systematically about 20% lower than the predictions.
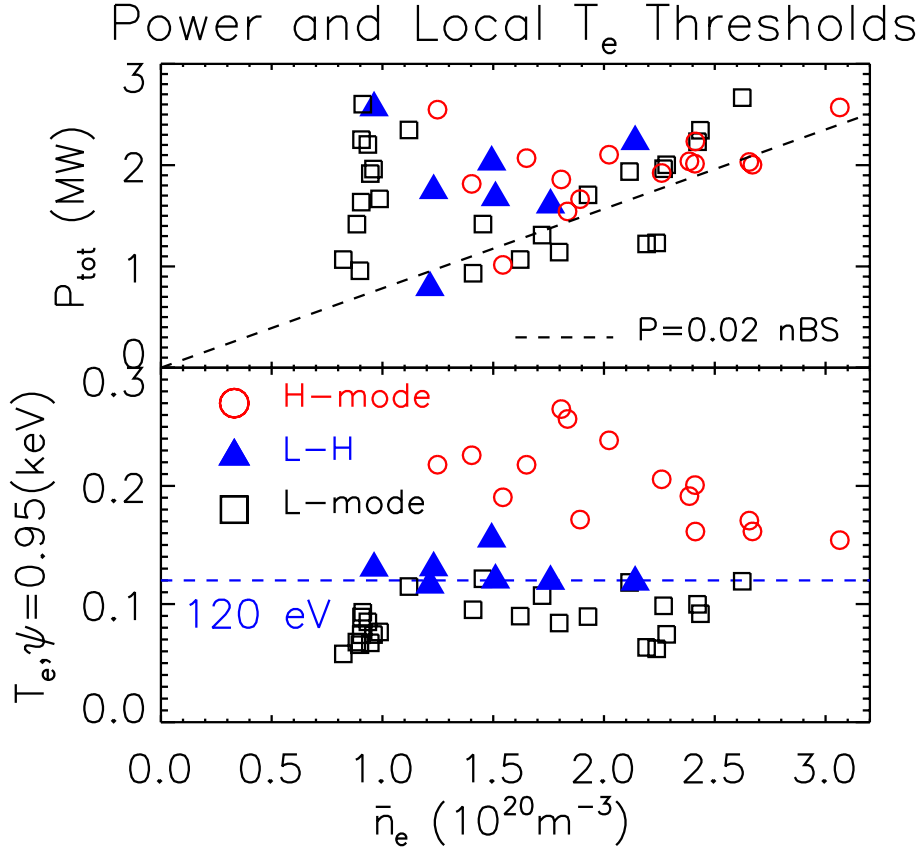
Power and Local T_e Thresholds

Figure 1. Total input power and edge electron temperature, plotted against line averaged density, for a series of discharges at fixed toroidal field (5.3 Tesla) and plasma current (0.8 MA). The triangles represent the data taken just before the plasma enters H-mode (denoted L-H); they occur at a constant temperature (in this case about 120 eV), while the global input powers under the same conditions show much more scatter.

Global energy confinement results, for both L- and H-mode plasmas, are displayed in figure 3, where they are plotted as a function of the ITER-89 L-mode confinement scaling. The L-mode discharges show good agreement with the scaling, and the H-mode plasmas have confinement enhancements of about a factor of 2. Two different sets of H-mode discharges are shown: ELM free, and a confinement mode which we call Enhanced D-Alpha H-Mode (EDA)[4,5]. The ELM free cases suffer from the typical problems of impurity accumulation accompanied by monotonically increasing core radiated power, followed by a collapse back to L-mode.[6] The EDA discharges, in contrast,
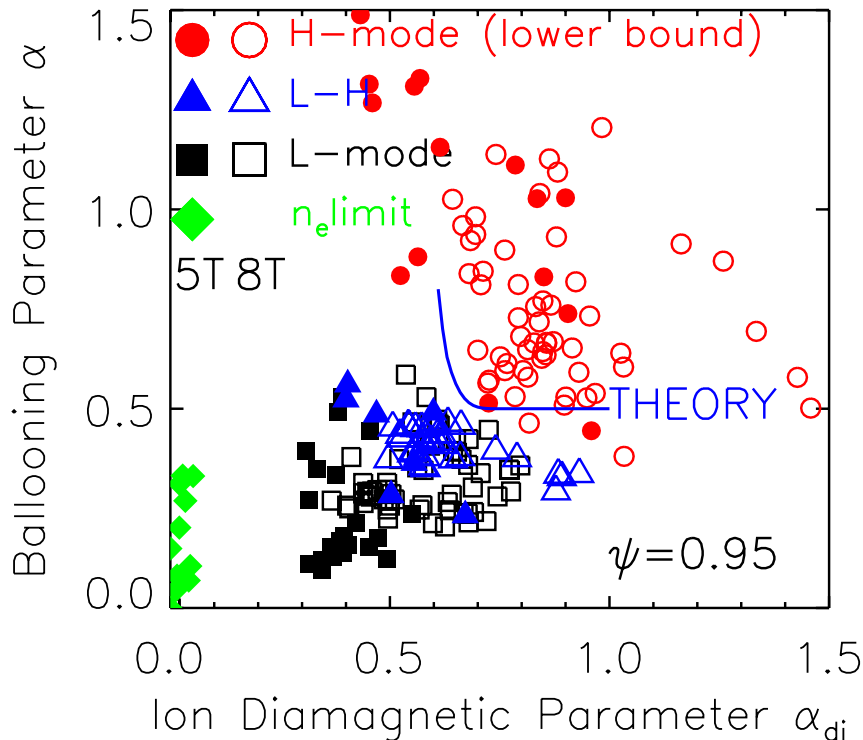
Figure 2. Edge pedestal parameters in L-mode (squares), just before the transition to H-Mode (triangles), and in developed H-modes (circles), plotted in the (α, α_{di}) plane. The theoretical boundary between L and H, from the theory of ref 3, is shown by the curve. Points corresponding to plasmas near the density limit, just before disruption, are shown in the lower left corner of the plot (diamonds).

show degraded impurity particle confinement, accompanied by an increase in edge density fluctuations, while the energy confinement is reduced by only about 10%. The EDA discharges can reach a steady-state, with $P_{rad}/P_{in} < 30\%$. Type I ELMS have not been observed in C-Mod, and the EDA regime does not suffer from large transient increases of heat and particle flux to the divertor. In some cases, typically when $\beta_N > 1.2$, small ELM activity is seen on top of the EDA. Studies examining the conditions that are more likely to produce EDA, rather than ELM free, indicate that EDA is favored at higher neutral pressure (or target plasma density), when $q_{95} > 3.5$, and when triangularity is in the range $.35 < \delta < .55$. Divertor geometry and baffling may also be important. The EDA appears similar to some H-modes that have been reported from other tokamaks, including the Low Particle Confinement Mode on JET[7], type II ELMs from DIII-D[8], and the small ELMs regime on JT60-U[9].

3. ICRF HEATING AND TOROIDAL ROTATION

Alcator C-Mod utilizes ICRF as its sole auxiliary heating method. Primarily relying on fundamental minority heating at $f = 80\,MHz$, up to $3.5\,MW$ is launched into
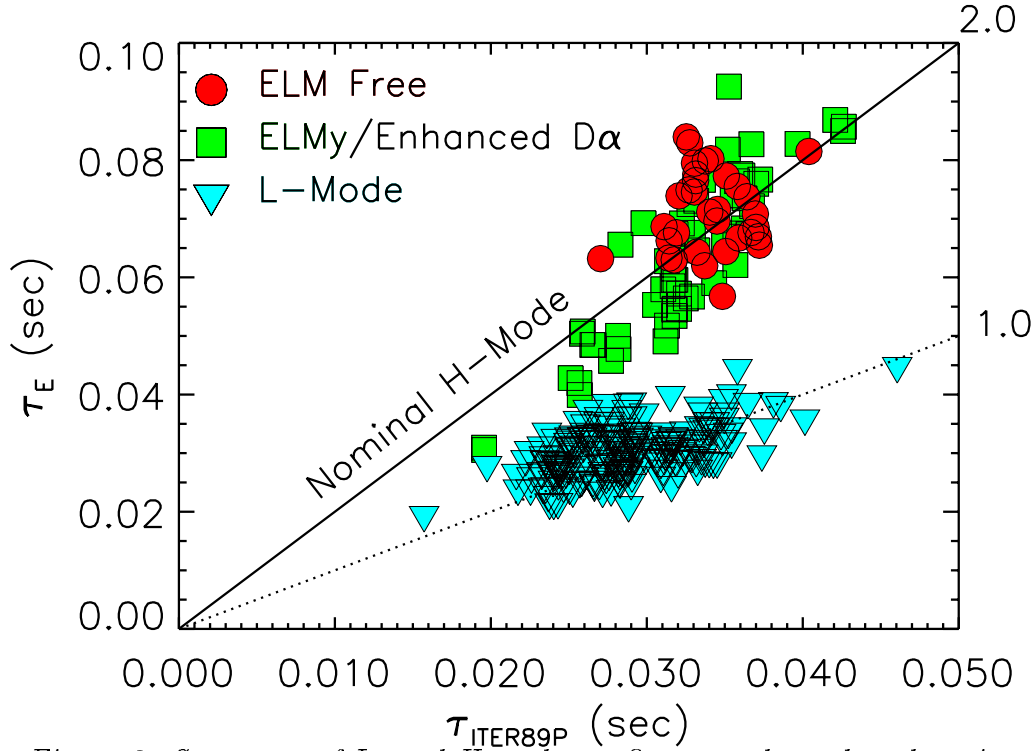
Figure 3. Summary of L- and H-mode confinement data plotted against the ITER-89P L-Mode scaling law. ELM-free H-Mode discharges are designated by the circles, and EDA H-Modes by the squares.

the plasma through 2 dipole antennas.[10] Efficient RF absorption has been measured both at $B = 5.4\,T$ (hydrogen minority), and at $8\,T$ (^{3}He minority), with 80% to 90% of the launched power going into plasma heating.[11] In contrast with neutral beam heating, the RF does not impart direct net momentum into the plasma, for the spectrum of waves launched. Nevertheless, rapid toroidal rotation is observed.[12] The rotation is seen in L-mode and H-mode plasmas, with the rotation velocity increasing with the total stored energy (W_{tot}) of the plasma (for fixed I_p), and decreasing with increasing current (for fixed W_{tot}). Rapid rotation is also seen in discharges with core transport barriers (PEP modes). The rotation is determined by measuring the Doppler shift in Ar^{+16} line radiation; the same instrumentation is used to simultaneously measure the argon ion temperature and density profiles. Profiles of the radial electric field can be inferred from these data, and one such result is shown in figure 4. The spectrometers are sensitive both to the toroidal and poloidal components of rotation, but the poloidal rotation, if present, is below the detectability of the system ($V_\theta < 3 \times 10^3\,m/s$), and the points shown in the figure are based on $E_r = \nabla P/neZ + V_\phi B_\theta$. The diamagnetic term is very small, because of the $1/Z$ dependence ($Z = 16$ in this case). Note that the calculated majority species diamagnetic term is not small, and the deuterium ion rotation, which is not measured, is expected to be about 1.5 times larger than that of the argon. Mach numbers, for argon, are of the order of 0.2, for the fastest rotation seen to date. The rotation profile is strongly peaked near the magnetic axis. Recent theoretical work suggests that ICRF heating of passing particles can result in a net inward shift of ions, which leads to a positive E_r and toroidal rotation in the co-current direction[13]. The

model correctly predicts the direction and magnitude of the rotation, and is qualitatively consistent with the observed axial peaking and dependence on plasma current.
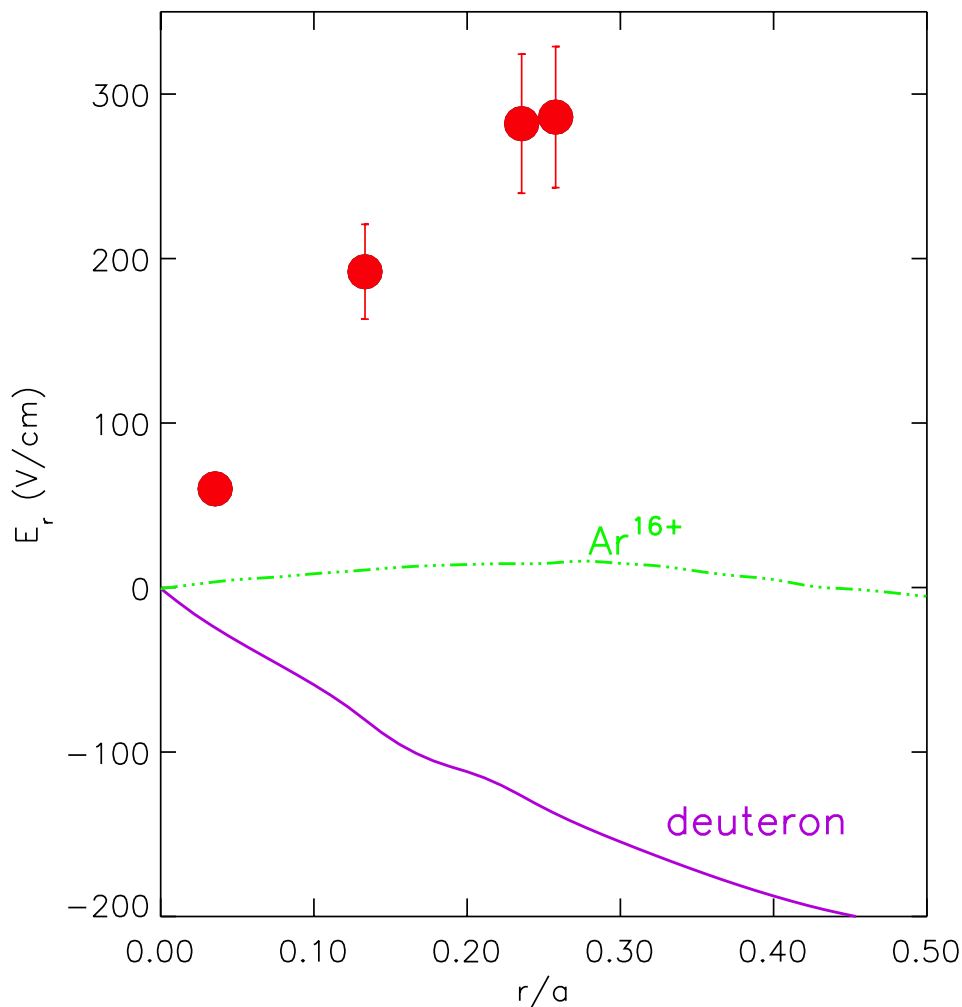

Figure 4. Radial electric field profile inferred from toroidal rotation measurements on Ar^{+16}. The diamagnetic contributions, calculated from the measured temperature and density profiles, are plotted for the argon ions (dash-dotted) and for the majority deuterons (solid line). The diamagnetic contribution for argon is very small, because of the $1/Z$ dependence of this term.

4. DIVERTOR STUDIES

In divertor research, we have implemented impurity injection feedback techniques to achieve quasi-steady-state detached divertor operation during EDA H-Mode plasmas. Using nitrogen, the peak divertor plate heat flux was reduced by about a factor of 5. Figure 5 shows the time histories for key plasma parameters in a typical case. Nitrogen puffing is started after the H-mode is established, and the puff rate is controlled with

active feedback using the radiated power measured with a bolometer viewing along a chord tangent to a radius just inside the last closed flux surface at the plasma midplane. As the plasma detaches, as indicated by the sharply decreasing heat flux to the outer divertor, the global energy confinement time drops by less than 10%, and the central Z_{eff} stays below 1.5. The minimal effect on the core is due, at least in part, to the high divertor compression of impurity gases ($C_Z = n_{Z,div}/n_{Z,core}$). C_Z increases with plasma density, giving high density operation an advantage. Parallel flows in the scrape-off are measured and appear to play a role in keeping C_Z high.

For detached plasmas, the strong reduction in ion current to the divertor target plate, as compared to attached conditions, is due to a combination of volumetric power loss in the SOL, plasma pressure loss along field lines and volume recombination of the ions. The importance of ion-neutral friction in reducing the target plate plasma pressure has been verified from parallel flow measurements of ionized and neutral species in the divertor using spectroscopic techniques. We have developed an analysis technique for determining the local volumetric recombination rate in detached regions, using the deuterium Balmer and Lyman series intensities. Opacities for the Lyman lines are measured, and the opacity effects reduce the overall recombination rates. The results show that recombination is significant, accounting for up to 75% of the ion sink during detachment, with the remainder recombining on the plate.

Measurements of particle balance in the main chamber and the divertor, combined with UEDGE [14] model calculations, indicate that under most operational conditions in C-Mod, the plasma in the scrape-off layer (SOL) surrounding the core plasma recycles by cross-field flow to the wall rather than by parallel flow into the divertor chamber. Figure 6 shows a compilation of data from a large number of discharges (both L-mode and H-mode). The open symbols show the plasma source in the main chamber (including core and main-chamber SOL), inferred from midplane Balmer-α measurements and the x symbols show the ion flux passing from the main chamber SOL into the divertor chamber, as measured with a Mach probe. The data are plotted against the neutral flux into the main chamber, inferred from midplane neutral pressure measurements combined with a free-streaming neutral model.[15] The remarkable result is that the main chamber recycling flux is always greater than that towards the divertor, usually by more than an order of magnitude. Modeling with the UEDGE transport code shows that in order to fit the measured scrape-off layer density profiles in this regime, some combination of a diffusion coefficient that rapidly grows with distance from the last-closed flux surface, or an inward particle pinch effect is required. An important implication is that the the neutral pressure at the midplane may be controlled more by the magnitude of the anomalous cross-field plasma transport rather than the geometry of the divertor or main chamber wall structures.

5. UPGRADES AND NEAR TERM PLANS

For the upcoming 1999 run campaign, several major facility and diagnostic upgrades are being implemented. The auxiliary heating capability of the machine is being doubled, with the addition of a 4-strap ICRF antenna. This will allow for the utilization of the full 8 MW complement of source power, which includes 4 MW at fixed
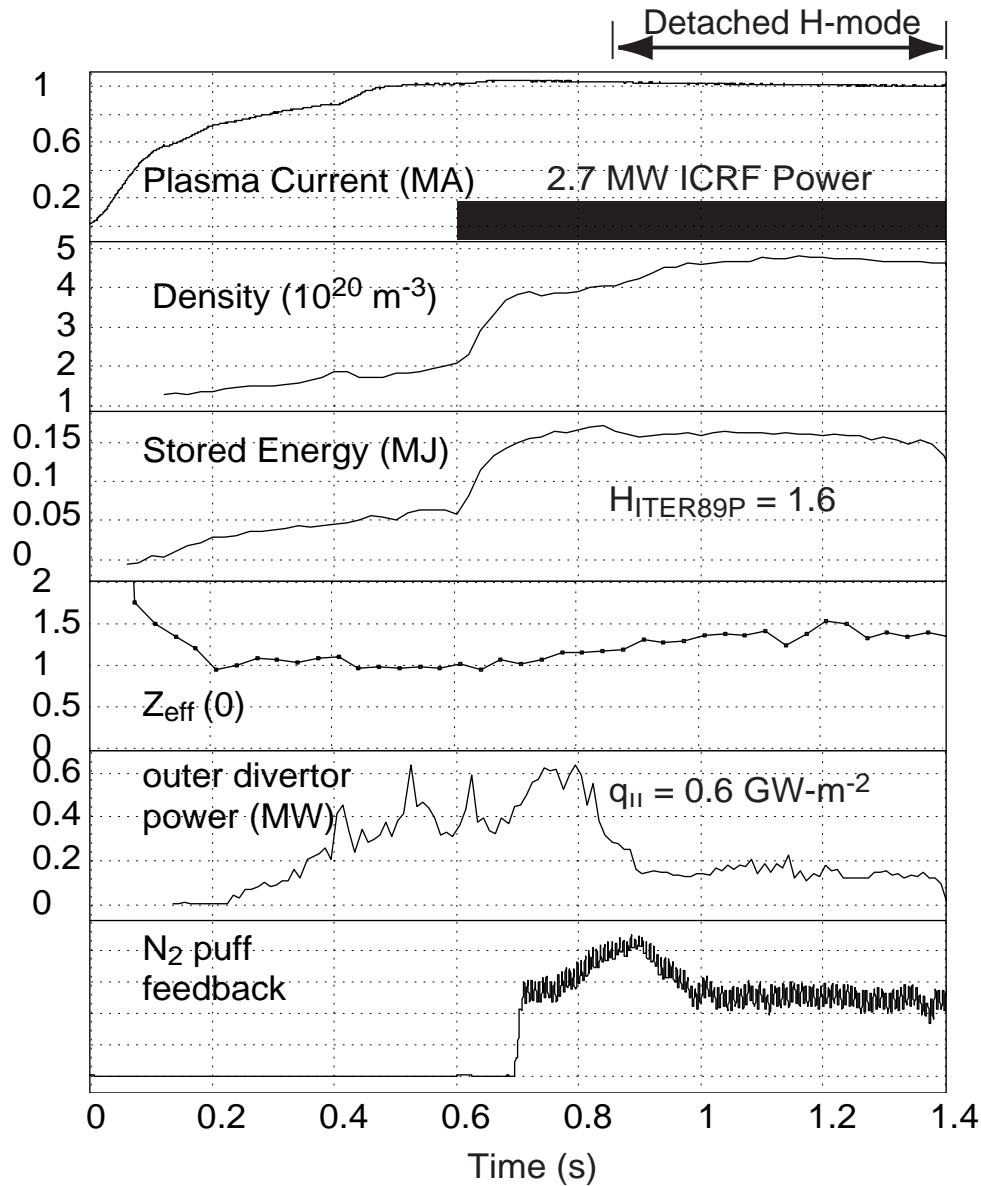
Figure 5. Time histories for several plasma parameters in a detached EDA H-Mode discharge. Note that after detachment (at about .82 s), Z_{eff} remains below 1.5, and the global energy confinement, as indicated by the stored energy, drops only slightly. Before the nitrogen puffing begins, the parallel power flow into the divertor in the scrape-off layer is $0.6\,GW/m^2$.
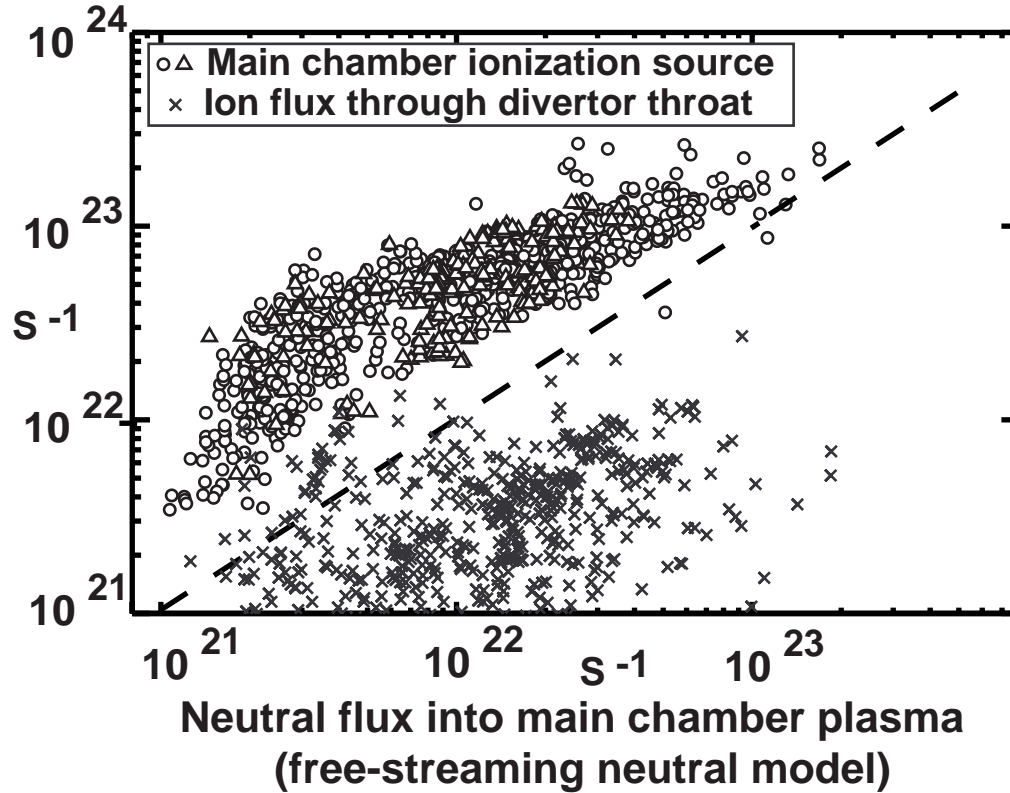
Figure 6. Comparison of the main chamber ionization source, measured from mid-plane Balmer-α brightness (open symbols) and ion flux through the divertor throat, measured with a scrape-off-layer fast scanning Mach probe (x symbols), plotted as functions of the neutral flux into the main chamber plasma, inferred from the main chamber neutral pressure. The results imply that the main chamber and divertor regions are largely isolated with respect to particle flows and recycling.

frequency (80 MHz), plus 4 MW tunable (42 to 78 MHz). Programmatic emphasis in this area for the run period will include investigations at higher β, increased divertor power loading, and continued investigations of H-mode and ELM physics. We will begin current drive investigation using both mode conversion and fast wave techniques, along with Bernstein Wave flow control. A diagnostic neutral beam is being added, along with associated diagnostics to measure ion temperature and rotation profiles through charge exchange recombination spectroscopy, fluctuations through beam emission spectroscopy, and current density profiles via the motional Stark effect. Additional diagnostic upgrades include ECE temperature fluctuation instrumentation, and better coverage of the pedestal region with high spatial resolution visible, x-ray, and bolometric imaging arrays, an edge Thomson scattering system and an improved reflectometer system. The outer divertor is being modified, with the addition of adjustable flow control "flappers", to allow for dynamic studies of the effects of variable neutral particle conduction between the divertor and the main chamber.
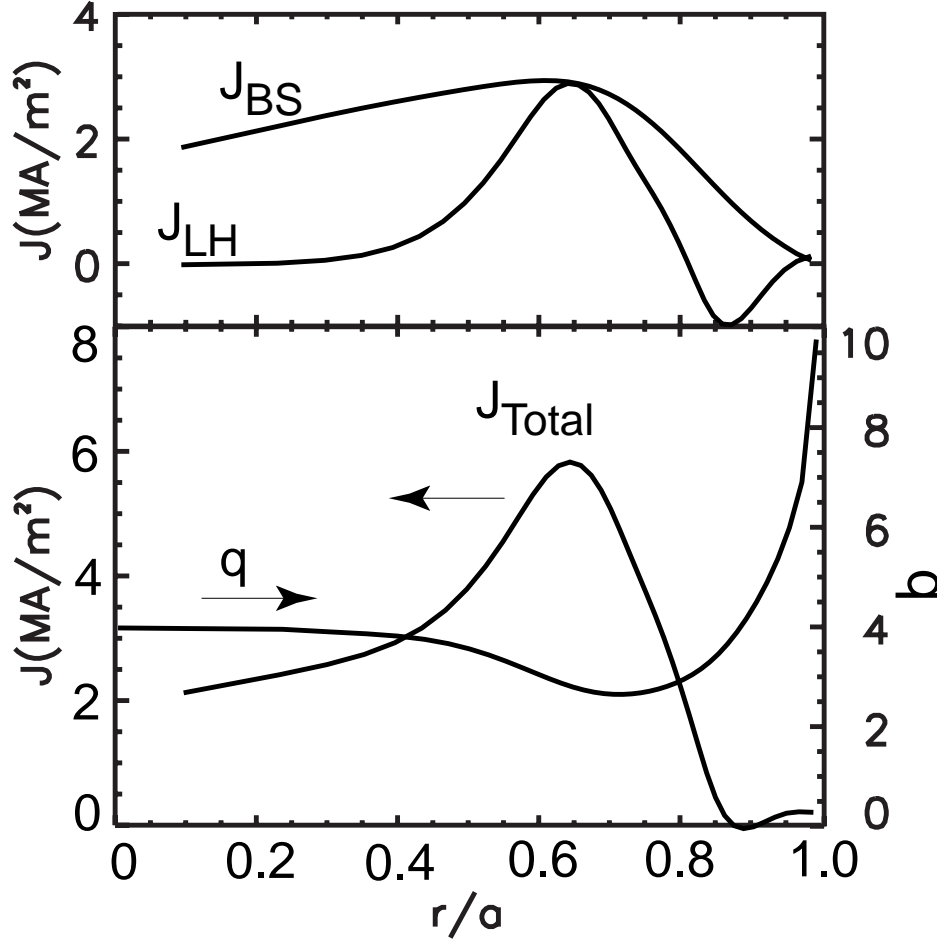
6. ADVANCED TOKAMAK RESEARCH

Figure 7. Modeled current density and q profiles for a steady state discharge with off axis lower hybrid current drive. In this case, the total current is 0.8 MA, with a bootstrap fraction of 70%.

Modeling of possible advanced tokamak operation on C-Mod has been undertaken with the ACCOME current drive and equilibrium code[16], combined with the PEST-II stability code[17]. For target plasmas with ICRF heating during the current ramp, characterized by inductively driven current profiles ($q_0 > 1$), it is found that reverse shear current density profiles can be created and maintained using off-axis Lower Hybrid Current Drive (LHCD). With the addition of 3 MW (absorbed) at 4.6 GHz, the modeling indicates that reverse shear plasmas at the β limit can be produced in C-Mod at $B_0 \sim$ 4.5 Tesla, $I_p \sim 0.8$ MA, and $\langle n_e \rangle$ in the range from 1×10^{20} to 2×10^{20} m^{-3}, with pulse length of about 10 skin times and 2 L/R times.[18] Figure 7 shows the resulting total steady state current density profile, as well as the components due to LHCD and bootstrap, the latter contributing about 70% of the total current. The q profile, also shown in the figure, has $r(q_{min}) \sim 0.7a$, and this radius can be controlled through variation of the RF power and wavenumber spectrum. The shaped C-Mod geometry ($\kappa \sim 1.7, \delta \sim 0.7$) results in high ideal MHD β-limits, even in the absence of a conducting shell ($\beta_N \leq 3.5$).

References:

[1] Hutchinson, et al., Phys. Plasmas, **1**(1994)1511.

[2] A.E. Hubbard, et al., PlasmaPhys. Contr. Fus. **40**(1998)689.

[3]B.N. Rogers and J.F. Drake, Phys. Rev. Lett. **79**(1997)229.

[4] Y. Takase, et al., Proc. 16th Int. Conf. Plasma Phys. Contr. Fusion, vol. I(1996)155

[5] J.A. Snipes, et al., Proc. 24th EPS, Berchtesgaden, **21A**, PartII(1997)565.

[6] ASDEX Team, Nucl. Fus. **29**(1989)1959.

[7] M. Bures, et al., Nucl. Fus. **32**(1992)539.

[8] T. Ozeki, et al., Nucl. Fus. **30**(1990)1425.

[9] Y. Kamada, et al., Plasma Phys. Cont. Fus. **38**(1996)1387.

[10] Y. Takase, et al., Phys. Plasmas **4**(1997)1647.

[11] S. Wukitch, et al., IAEA-CN-69-CDP/10, these procedings.

[12] J. Rice, et al., Nucl. Fus. **38**(1998)75.

[13] C.S. Chang, et al., IAEA-CN-69-THP/34, these procedings]

[14] T.D. Rognlien, et al., J. Nucl. Mat. **196-198**(1992)347.

[15] M.V. Umansky, etal., Phys. Plasmas **5**(1998)3373.

[16] R.S. Devoto, et al., Nucl. Fusion **32**, (1992) 773.

[17] R.C. Grimm, et al., J. Computational Physics **49** (1983)49.

[18] P.T. Bonoli, et al., Plasma Phys. Cont. Fusion **39**, (1997) 223.